ACS APPLIED MATERIALS & INTERFACES

Research Article

www.acsami.org

Reducing Exciton Binding Energy by Increasing Thin Film Permittivity: An Effective Approach To Enhance Exciton Separation Efficiency in Organic Solar Cells

Sibel Y. Leblebici,[†,‡] Teresa L. Chen,[†] Paul Olalde-Velasco,[§] Wanli Yang,[§] and Biwu Ma*[,†,#]

[†]The Molecular Foundry, Lawrence Berkeley National Laboratory, Berkeley, California 94720, United States

[‡]Department of Materials Science & Engineering, University of California, Berkeley, California 94720, United States

[§]The Advanced Light Source, Lawrence Berkeley National Laboratory, Berkeley, California 94720, United States

[#]Department of Chemical & Biomedical Engineering, Florida State University, Tallahassee, Florida 32310, United States

Supporting Information

ABSTRACT: Photocurrent generation in organic solar cells requires that excitons, which are formed upon light absorption, dissociate into free carriers at the interface of electron acceptor and donor materials. The high exciton binding energy, arising from the low permittivity of organic semiconductor films, generally causes low exciton separation efficiency and subsequently low power conversion efficiency. We demonstrate here, for the first time, that the exciton binding energy in B,O-chelated azadipyrromethene (BO-ADPM) donor films is reduced by increasing the film permittivity by blending the BO-ADPM donor with a high dielectric constant small molecule, camphoric anhydride (CA). Various spectroscopic techniques, including impedance spectroscopy, photon absorption and emission spectroscopies, as well as X-ray spectroscopies, are applied to characterize the thin film electronic and photophysical properties. Planar heterojunction solar cells are fabricated with a BO-ADPM:CA film as the electron donor and C_{60} as the acceptor. With an increase in the dielectric constant of the donor film from ~4.5 to ~11, the exciton binding energy is reduced and the internal quantum efficiency of the photovoltaic cells improves across the entire spectrum, with an ~30% improvement in the BO-ADPM photoactive region.

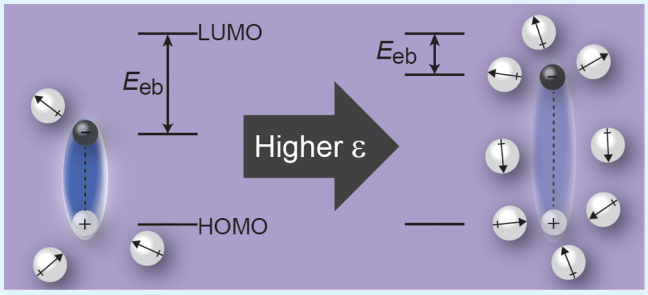

KEYWORDS: *exciton binding energy, exciton separation efficiency, organic solar cells, permittivity, small molecule electron donor*

INTRODUCTION

The power conversion efficiencies (PCEs) of organic solar cells (OSCs) reported in literature have increased significantly over the last few decades from ~1% to more than 10%.[1−9] These remarkable advances have been driven by tremendous efforts in understanding the OSC device operation and developing new materials and architectures. Nevertheless, the PCEs of OSCs lag behind those of their inorganic counterparts due in part to the intrinsic properties of organic semiconductors. Organic semiconductors generate Frenkel excitons, Coulombically bound electron-hole pairs with relatively high exciton binding energies (E_{eb}) due to their low dielectric constant, the presence of significant electron-lattice interactions, and electron correlation effects.[10,11] The excitons that diffuse to the donor/acceptor interface separate into free carriers provided that the energy offset between the lowest unoccupied molecular orbital (LUMO) levels of the donor and the acceptor (ΔLUMO) is sufficient to overcome E_{eb}.[12−14] The efficiency of photocurrent generation as a function of photon wavelength, the external quantum efficiency (EQE), is a product of the efficiencies of the photocurrent generation steps as shown in Figure 1 and described by eq 1,

$$\eta_{EQE} = \eta_A \eta_{IQE} = \eta_A \eta_{ED} \eta_{ES} \eta_T \eta_{CC} \quad (1)$$

where η_A is the photon absorption efficiency, η_{IQE} is the internal quantum efficiency (IQE), η_{ED} is the exciton diffusion efficiency, η_{ES} is the exciton separation efficiency, η_T is the carrier transport efficiency, and η_{CC} is the carrier collection efficiency.

It is generally assumed that a sufficiently large ΔLUMO is needed for efficient exciton separation; however, a large ΔLUMO is also undesirable because it results in a low open circuit voltage (V_{oc}).[15] A highly promising approach to circumvent this limitation is to reduce the E_{eb} of the electron donor layer, thereby simultaneously achieving efficient η_{ES} and large V_{oc} and thus realizing enhanced EQEs and PCEs for OSCs. Other approaches to increase the exciton separation

Received: July 10, 2013
Accepted: September 16, 2013
Published: September 16, 2013

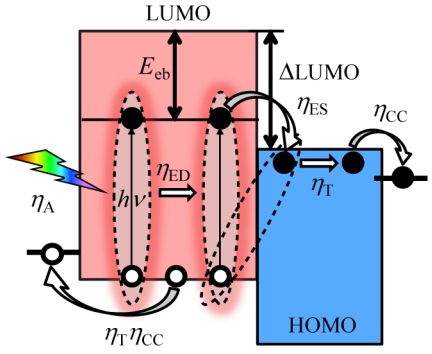

Figure 1. Photocurrent generation occurs in several steps in OSCs, each having its own efficiency. The steps in sequential order are light absorption (η_A), exciton diffusion (η_{ED}), exciton separation (η_{ES}), carrier transport (η_T), and carrier collection (η_{CC}). η_{ES} is a function of the difference between the exciton binding energy, E_{eb}, and the donor−acceptor LUMO offset, ΔLUMO.

efficiency include adding ferroelectric polymers,[16,17] applying an external electric field,[18] and p-type doping.[19]

The exciton binding energy is directly related to the Coulombic potential between the electron and hole,

$$E_{eb} = e^2/4\pi\varepsilon_0\varepsilon_r r \quad (2)$$

where e is the elementary charge, ε_0 is the permittivity of vacuum, ε_r is the permittivity of the material, and r is the distance between the electron and hole. Equation 2 is a component of the Bethe Salpeter equation, which is used to calculate the exciton binding energy in organic semiconductors.[20] As a result, eq 2 has important implications for how permittivity affects exciton binding energy. Typical organic semiconductors have a permittivity of $\varepsilon_r \sim 3-4$,[21] resulting in exciton binding energies of 0.3−1 eV,[10,22−25] which are significantly higher than those of inorganic semiconductors, e.g., ∼10 meV for silicon with a permittivity of 12.[11] According to eq 2, increasing the permittivity should lead to a reduction in E_{eb}. To this end, Engel et al. have demonstrated an increase in free carrier generation in pentacene as a result of depositing it on high dielectric constant substrates[21] and, to push the limits of organic photovoltaics, methods to increase the permittivity of organic semiconductors have become increasingly important.[26,27]

Herein, we demonstrate a very simple approach to lowering E_{eb} in organic thin films by blending a solution-processable donor molecule, B,O-chelated azadipyrromethene (BO-ADPM), with a high dielectric constant molecule, camphoric anhydride (CA). The molecular structures are shown in Figure 2a and the band gap alignment is shown in the Supporting Information Figure S1. The major advantages of BO-ADPM are its intense broad absorption and narrow band gap of 1.5 eV, which affords photocurrent generation in the near-infrared region when coupled with the acceptor C_{60}.[28] However, the EQE values of the BO-ADPM/C_{60} system are low, which is partially due to the insufficient ΔLUMO to overcome E_{eb}, leading to a low η_{ES}. This system, therefore, serves as a model platform to study the effect of film permittivity on E_{eb} and η_{ES}.

MATERIALS AND METHODS

The synthesis and characterization of BO-ADPM has previously been reported.[28] Polystyrene (PS), CA, sublimed grade C_{60}, and bathocuproine (BCP) were purchased from Aldrich. Pre-patterned indium tin oxide (ITO)-coated glass substrates were purchased from Thin

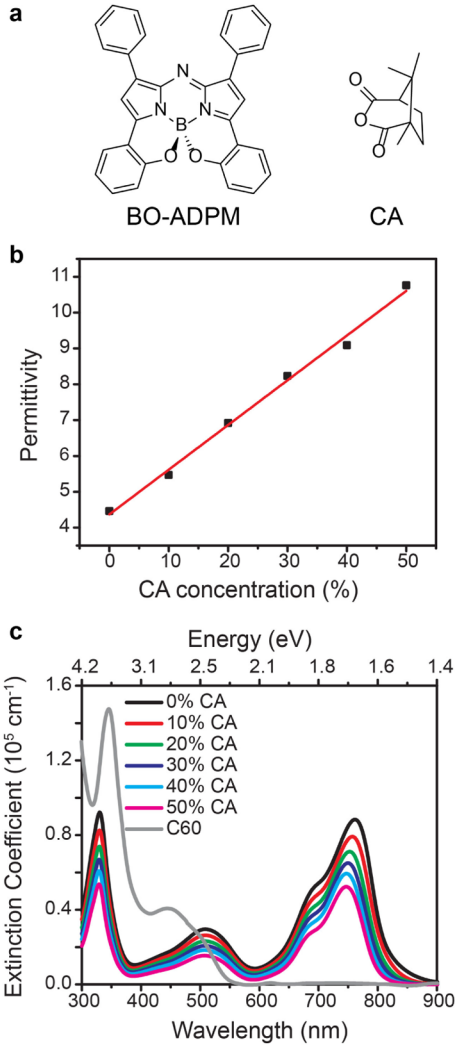

Figure 2. (a) Molecular structures of the active donor material BO-ADPM and highly polar molecule CA. (b) Plot of the relationship between the concentration of CA in blended BO-ADPM:CA films and the permittivity of the thin film. The line is a linear fit to the data points. (c) UV−visible absorption spectra of BO-ADPM:CA blend films at various weight ratios and C_{60}.

Film Devices, Inc. Poly(3,4-ethylenedioxythiophene):poly(styrenesulfonate) (PEDOT:PSS) (Baytron PH 500) was purchased from H. C. Starck. BO-ADPM:CA films were prepared by spin-casting mixtures of BO-ADPM and CA films dissolved in tetrahydrofuran (THF) at the appropriate ratios to create films with 10, 20, 30, 40, and 50 wt % CA. Both BO-ADPM and CA are highly soluble in THF and the solutions were spin-cast within 24 h of forming the solution. OSCs were fabricated in a planar heterojunction structure of ITO/PEDOT:PSS(30 nm)/BO-ADPM:CA(20 nm)/C_{60}(35 nm)/BCP(8 nm)/Ag(100 nm). Control devices had a similar structure of ITO/PEDOT:PSS/BO-ADPM:PS/C_{60}(35 nm)/BCP(8 nm)/Ag(100 nm), where the CA has simply been replaced by PS for each weight ratio.

Devices were fabricated in the following steps. ITO-coated glass substrates were cleaned by successive sonication in soap solution, deionized water, acetone, and isopropyl alcohol for 15 min at 40 °C and UV ozone cleaned for 10 min. PEDOT:PSS was spin-cast onto the cleaned ITO coated glass substrate and baked at 140 °C for 20 min. BO-ADPM:CA and BO-ADPM:PS solutions in THF (2 mg/mL) were spin-coated onto the PEDOT:PSS film at 2000 rpm for 60 s. Subsequently, C_{60}, BCP, and Ag were thermally evaporated under high vacuum (∼2×10^{-6} mbar) at rates of 1, 1, and 2 Å s^{-1}, respectively. The Ag electrodes defined the devices with a shadow mask of 0.03 cm^2 in

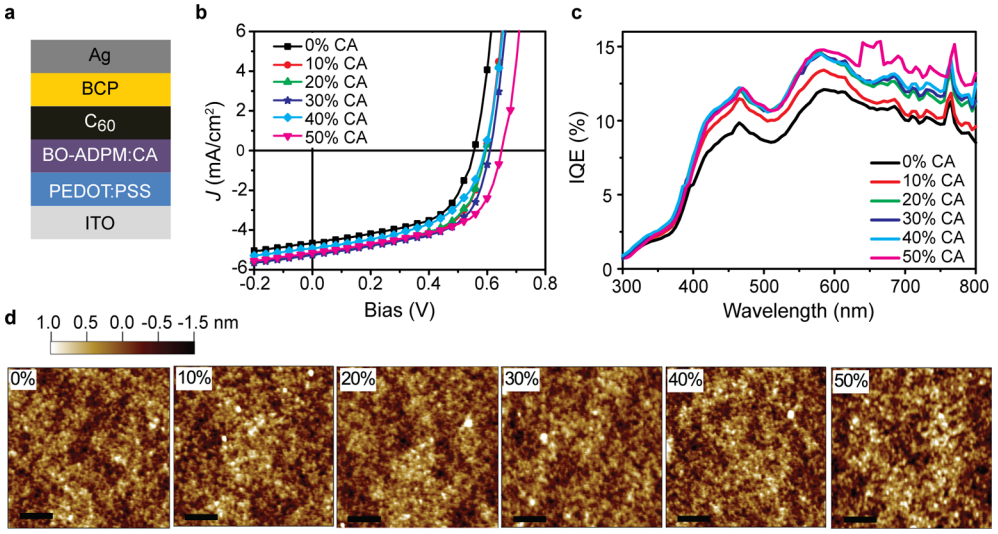

Figure 3. (a) BO-ADPM:CA/C_{60} photovoltaic device structure. (b) Current density−voltage (J−V) curves of the highest efficiency BO-ADPM:CA/C_{60} devices of 6 devices. (c) IQE spectra calculated from reflectance and EQE spectra demonstrating an increase in IQE with increasing CA concentration. (d) Tapping-mode AFM images of BO-ADPM:CA blend films with 10%, 20%, 30%, 40%, 50% CA have root-mean-square roughness of 0.31, 0.33, 0.31, 0.34, and 0.37 nm, respectively. The scale bar represents 1 μm.

area. Additionally, PS:CA matrix films of varying weight ratios were doped with constant weight percent of BO-ADPM to observe shifts in the optical band gap in the absence of BO-ADPM aggregation effects. These films were prepared by spin-casting solutions of PS and CA in THF mixed to form 10, 20, 30, 40, and 50 CA wt % solutions with a constant 0.05 wt % BO-ADPM.

Permittivity was measured via impedance spectroscopy of parallel plate capacitors with the structures ITO/BO-ADPM:CA or PS:CA:BO-ADPM (~200 nm)/Au(70 nm) using a Solartron SI 1260 Impedance−Gain/phase Analyzer at an AC level of 0.1 V and no DC bias. The calculation of the permittivity from the impedance spectroscopy measurement is described in the Supporting Information.

UV−visible absorption measurements of the thin films were conducted with a CARY 5000 UV-Vis-NIR spectrophotometer. Spectral reflectance of the full devices for IQE calculations was measured using a CARY 5000 Internal Diffuse Reflectance accessory with an integrating sphere and a polytetrafluoroethylene reference. Photoluminescence (PL) and PL lifetime were measured using a Horiba Nanolog Spectrofluorometer in a nitrogen protecting environment.

The current density−voltage (J−V) curves were measured with a Thermal-Oriel 300 W solar simulator with AM 1.5G solar illumination at 100 mW cm^{-2} and a Keithley 236 source-measure unit. EQE spectra were measured with a monochromator and calibrated with a silicon photodiode up to 800 nm. Hole-only devices to determine hole mobility in the BO-ADPM:CA films were fabricated with the structure of ITO/PEDOT:PSS/BO-ADPM:CA/Au.

X-ray emission spectroscopy (XES) and x-ray absorption spectroscopy (XAS) measurements were conducted at the Advanced Light Source undulator beamline 8.0.1. BO-ADPM:CA films (100 nm) were formed by spin-casting solutions onto Si substrates. We performed a comparative study to address radiation damage concerns. Reliable data were collected with the samples cooled to 90 K by liquid nitrogen and a defocused X-ray beam with a minimum photon dose. In particular, for the lengthy XES measurements, samples were kept itinerary with a programmed motor on a stable cryostat, to prevent the X-ray beam from remaining stationary on the sample surface. Additionally, XAS was remeasured on a spot along the itinerary path of the sample motion after the XES measurement to confirm the samples are free of radiation damage. XAS spectra were collected in both total electron and total florescence yield modes, which correspond to a probe depth of several nanometers and about 100 nm, respectively. XES spectra were collected through a Rolland circle soft X-ray spectrometer. The experimental resolution of XES and XAS is about 200 and 80 meV, respectively, but the energy position of the spectral leading edges is defined with much better precision, which is typical for soft X-ray spectroscopy. The XES and XAS data shown are normalized to collection time and photon flux monitored by a clean gold mesh. Excitation energy for performing the XES experiments was high above the absorption edge at 310 eV to avoid any resonance effects.

Atomic force microscopy (AFM) images were recorded on a Veeco Nanoscope scanning probe microscope in tapping mode for spin-coated BO-ADPM:CA films on PEDOT:PSS coated ITO/glass substrates. All film thicknesses were measured using a Dektak 150 profilometer.

RESULTS AND DISCUSSION

The effect of the CA concentration on the permittivity of the blends of BO-ADPM and CA was studied using impedance spectroscopy. The high solubility and low crystallinity of both BO-ADPM and CA allowed uniform thin films to be prepared via solution processing. As shown in Figure 2b, the film's dielectric constant at an AC frequency of 1000 Hz increases linearly with CA wt % from 4.46 for the neat BO-ADPM film to 10.8 for the film with a 1:1 blend ratio. This is similar to the literature reported tuning of the permittivity in red dye DCM2:PS thin films upon CA doping.[29] Permittivity as a function of frequency for each CA concentration is available in the Supporting Information Figure S2. Blending BO-ADPM with CA also resulted in a significant reduction of the film absorption properties, as the high band gap CA molecule does not absorb in the visible light region. Figure 2c shows the linear decrease in absorption intensity with the increasing wt% of CA blend films and resulting decrease in BO-ADPM content.

Planar heterojunction OSCs were fabricated with solution-processed neat BO-ADPM and blended BO-ADPM:CA thin films as the donor and vapor-deposited C_{60} as the acceptor, with a structure of ITO/PEDOT:PSS(30 nm)/BO-ADPM:CA-(20 nm)/C_{60}(35 nm)/BCP(8 nm)/Ag(100 nm), shown in Figure 3a. The J−V curves shown in Figure 3b represent the highest efficiency device at each BO-ADPM:CA ratio and the average device characteristics of 6 devices at each ratio, including short circuit current density (J_{sc}), V_{oc}, fill factor (FF), and PCE are listed in Table 1. The PCE of the 50:50

dx.doi.org/10.1021/am402744k | ACS Appl. Mater. Interfaces 2013, 5, 10105−10110

Table 1. Photovoltaic Performance Parameters Taken as an Average of 6 Devices Including the Standard Deviation and Hole Mobilities of BO-ADPM:CA Donor Blend Solar Cells with Different Weight Ratios of CA

BO-ADPM:CA weight ratio	V_{oc} (V)	J_{sc} (mA/cm^2)	FF (%)	PCE (%)	hole mobility (cm^2/(V s))
100:0	0.550 ± 0.006	−4.65 ± 0.13	52.6 ± 4.6	1.34 ± 0.10	4.06×10^{-5}
90:10	0.599 ± 0.005	−4.83 ± 0.26	55.4 ± 1.7	1.61 ± 0.12	-
80:20	0.587 ± 0.015	−4.96 ± 0.15	54.8 ± 1.7	1.60 ± 0.07	1.05×10^{-6}
70:30	0.616 ± 0.007	−4.95 ± 0.26	56.3 ± 0.7	1.72 ± 0.10	-
60:40	0.628 ± 0.017	−4.61 ± 0.19	54.3 ± 1.7	1.57 ± 0.03	2.11×10^{-7}
50:50	0.646 ± 0.022	−4.41 ± 0.42	49.6 ± 7.7	1.43 ± 0.35	-

devices has a large standard deviation because the mixing is not uniform at such high concentrations of CA. As a result, higher concentrations of CA were not investigated. The results of the BO-ADPM:CA donor devices are contrasted to the BO-ADPM:PS control device data shown in Supporting Information Figure S3. The control devices have the same structure as the BO-ADPM:CA devices, but the higher permittivity CA is replaced by the low permittivity (2.7) PS polymer for each weight ratio. In the BO-ADPM:PS devices, no change was observed in the V_{oc} upon increased concentration of PS in the donor film and the J_{sc} dropped significantly with increased PS concentration. It is important to note that all the BO-ADPM:CA devices showed similar J_{sc} values between 4.66 and 5.26 mA cm^{-2}, although they possess notably different absorption efficiencies (η_A), as shown in Figure 2c. The relatively constant J_{sc} upon decreased η_A suggests an increase in IQE by the improvement of one or more of the remaining photocurrent generation processes, i.e., η_{ED}, η_{ES}, η_T, η_{CC}. To confirm this, IQE spectra were calculated from EQE and reflectance spectra, see Supporting Information Figure S4. Indeed, upon increasing the CA concentration, the IQE spectra (Figure 3c) show a clear enhancement throughout the entire spectrum from 300 to 800 nm where BO-ADPM absorbs light and contributes to photocurrent. The dissociation efficiency of excitons generated in C_{60} is also expected to increase slightly due to the increased dielectric constant at the interface with the BO-ADPM:CA donor. Note that the contributions to the IQE from C_{60} and BO-ADPM are difficult to decouple except in the 600−800 nm region, where only the BO-ADPM component contributes to the photocurrent generation—the improvement in the IQE is seen most clearly in this region. In the BO-ADPM:CA devices, the increase in V_{oc} with increased CA concentration is attributed to the increase in the dipole moment at the interface between the BO-ADPM:CA and C_{60} layers.[16,30] A detailed investigation is ongoing to understand the change in dipole moment at that interface.

We studied each photocurrent generation process described in eq 1 to determine which are responsible for the increase in IQE. First, the hole carrier mobilities of the BO-ADPM:CA films were determined via space-charge limited current measurements, with mobility values listed in Table 1. As expected, a greater weight percent of CA, a non-conducting molecule, in the blended film resulted in lower mobility in the BO-ADPM:CA films and reduced hole transport efficiency. Electron transport efficiency is considered constant, since the same acceptor layer of C_{60} was used for all the devices. Thus, it is likely that both η_{ED} and η_T worsened or stayed constant, preventing their contribution to the observed increase in IQE. Moreover, because the same electrodes were used, η_{CC} is believed to be very similar for all the devices. Therefore, the only remaining photocurrent generation process that could possibly be responsible for the increase in IQE is η_{ES}. η_{ES} is influenced by both the morphological and electronic properties of the donor−acceptor interface. Greater surface roughness of the donor film in planar heterojunction devices creates a larger donor−acceptor interfacial area, allowing for more exciton separation sites and higher η_{ES}.[31,32] But this is not the case for the BO-ADPM:CA devices. AFM images in Figure 3d show that the film topology is not altered by the incorporation of CA, and that the films are extremely smooth, i.e., a root-mean-square roughness of 0.31 nm for the BO-ADPM neat film and 0.37 nm for the film with 50% CA. Thus, the observed increase in IQE is not believed to be a result of greater donor−acceptor interfacial area from morphological changes.

By process of elimination, the only remaining photocurrent generation process contributing to the enhancement of IQE is η_{ES} resulting from the difference between ΔLUMO and E_{eb}. Provided that CA is not chemically bonding to BO-ADPM in the blended films, negligible changes to the BO-ADPM highest occupied molecular orbital (HOMO) and LUMO levels are expected. To confirm this hypothesis, we performed synchrotron-based XAS and XES, which probe the LUMO and HOMO states respectively. For organic semiconductors, the combination of XAS and XES has been demonstrated to be effective in probing the conduction and valence states.[33−35] We compared the XAS and XES spectra collected on neat BO-ADPM and 50:50 ratio BO-ADPM:CA films. Figure 4a shows that the leading edges of the XAS spectra, which correspond to the LUMO states, remain exactly the same for both the neat BO-ADPM and BO-ADPM:CA 50:50 films. XES experiments, however, require a high X-ray dose and could cause radiation damage when studying organic compounds.[33−35] We thus performed a comprehensive study on radiation damage (Supporting Information Figures S5 and S6) and collected reliable XES spectra with a defocused X-ray beam on an itinerary sample surface cooled to liquid nitrogen temperature. Although the features in the XES spectra in Figure 4b are broad due to the intrinsically low count rate of such a technique, the XES leading edges, which correspond to the HOMO states of the two systems, are at the same energy. Analysis on the detailed lineshape of the XES and XAS spectra is not a topic of this work; nonetheless, the soft XES and XAS data strongly suggest that the HOMO and LUMO levels do not change upon addition of CA into the film.

Absorption and PL spectroscopy were employed to determine the change in E_{eb}. Although absorption spectroscopy is commonly used to estimate the energy of the HOMO-LUMO gap, or transport gap (E_T), of organic semiconductors, it is actually a measure of the optical band gap, E_{op}.[36,37] The optical band gap and transport gap differ by E_{eb}, $E_{eb} = E_T - E_{op}$. The normalized absorption spectra of the BO-ADPM:CA blend films are shown in Figure 5a; the blue-shift in the lowest energy absorption peak demonstrates a 32.7 meV increase in E_{op}, which suggests that E_{eb} decreased by 32.7 meV. It is important

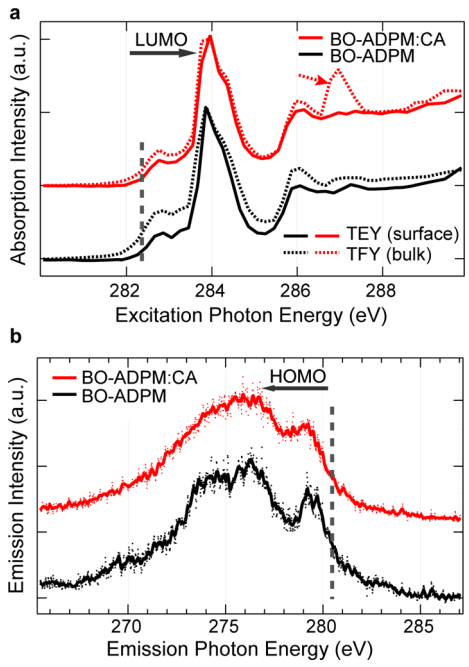

Figure 4. (a) X-ray absorption spectroscopy measured in total electron yield (TEY) and total fluorescence yield (TFY) modes provide information about the surface and bulk of the film, respectively. The LUMO levels of BO-ADPM and BO-ADPM:CA (50:50 wt %) are shown to be identical with same edge onset energy. The peak at 287 eV indicates a composition variation between the surface and the bulk of the BO-ADPM:CA film. (b) X-ray emission spectroscopy demonstrates that the edge onset does not differ between neat BO-ADPM and with 50% CA doping. The solid lines are smoothed data.

to note that the blue-shift in the absorption spectra could be partially due to reduced intermolecular $\pi-\pi$ interactions as a result of decreased BO-ADPM concentration in the film.

To eliminate $\pi-\pi$ interaction effects and ensure that the peak shift is in part due to the change in permittivity of the film, absorption and PL spectroscopy of PS:CA films doped with a low and constant concentration of 0.5% BO-ADPM were measured. In the BO-ADPM doped PS:CA film absorption and PL spectra (Figure 5b,c), a blue-shift of ~7 meV was observed in the absence of BO-ADPM $\pi-\pi$ interactions. Unfortunately, the addition of PS significantly reduces the enhancing effect of CA on the permittivity of the film. The BO-ADPM doped PS film without CA has a permittivity of 2.73, which increases to only 5.74 for the doped PS film with 40% CA (see Supporting Information Table S2); this is much lower than the permittivity of BO-ADPM:CA films without PS. The PL quantum efficiency decreases and the exciton lifetime does not change significantly upon the increase of CA concentration, indicating increased nonradiative decay and decreased radiative decay rates, as shown in Supporting Information Figure S7. This is not surprising, as the energy shift of the lowest excited state could lead to a higher intersystem cross rate, which quenches the emission.[38] These findings support the observed decrease of E_{eb} with increasing film dielectric constant, which leads to higher exciton separation efficiency, though it is difficult to decouple $\pi-\pi$ interaction and permittivity effects.

CONCLUSION

In summary, we have demonstrated the enhancement of exciton separation efficiency by decreasing the exciton binding

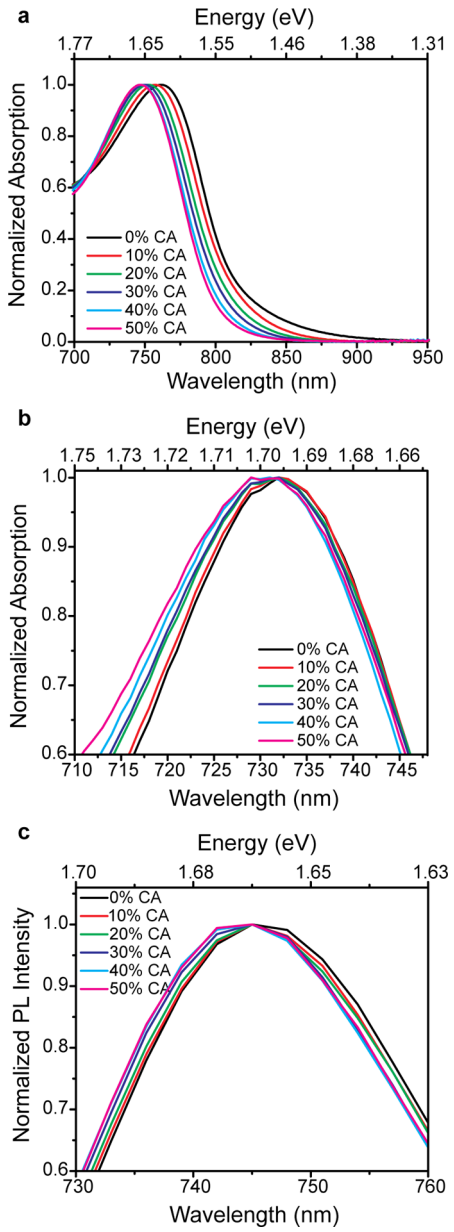

Figure 5. (a) Normalized absorption spectra of BO-ADPM:CA films, (b) normalized absorption spectra of PS:CA films doped with BO-ADPM, and (c) normalized PL spectra of PS:CA films doped with BO-ADPM show a blue-shift with increasing CA concentration.

energy in operating organic solar cells. The reduced exciton binding energy was realized by increasing the film permittivity and decreasing the intermolecular $\pi-\pi$ interactions, i.e., blending the electron donor BO-ADPM with a high dielectric constant small molecule CA. An increase in IQE across the entire spectrum was achieved, with a 30% increase in IQE at λ= 770 nm, by increasing the dielectric constant of the donor film from 4.46 to 10.8. Our findings suggest organic semiconductors with high permittivity have great potential in improving the power conversion efficiency of organic solar cells. We are currently pursuing further studies with other small molecule systems, which should prove insightful as to the application of this approach. The concept of reducing the exciton binding energy could be especially meaningful for OSCs with low band gap materials, where the LUMO energy offset is often minimized.

■ ASSOCIATED CONTENT

Supporting Information

Band gap alignment of materials used in photovoltaic devices; permittivity as a function of frequency and the permittivity calculations; control device results; EQE and reflectance spectra for the calculation of IQE; results of XAS and XES radiation damage tests; permittivity, PL intensity, and PL lifetime of PS:CA films doped with BO-ADPM. This material is available free of charge via the Internet at http://pubs.acs.org.

■ AUTHOR INFORMATION

Corresponding Author

*Biwu Ma, Department of Chemical & Biomedical Engineering, Florida State University, Tallahassee, Florida 32310 (USA), E-mail: bma@fsu.edu.

Notes

The authors declare no competing financial interest.

■ ACKNOWLEDGMENTS

Work at the Molecular Foundry and the Advanced Light Source, Lawrence Berkeley National Laboratory, was supported by the Office of Science, Office of Basic Energy Sciences, of the U.S. Department of Energy under Contract No. DE-AC02-05CH11231. This material is also based upon work supported by the National Science Foundation Graduate Research Fellowship under Grant No. (NSF DGE 1106400). B. Ma thanks Florida State University for the startup fund support through the university Energy & Materials Initiative.

■ ABBREVIATIONS

PCE, power conversion efficiency
OSC, organic solar cell
E_{eb}, exciton binding energy
LUMO, lowest unoccupied molecular orbital
EQE, external quantum efficiency
IQE, internal quantum efficiency
V_{oc}, open circuit voltage
BO-ADPM, B,O-chelated azadipyrromethene
CA, camphoric anhydride
BCP, bathocuproine
ITO, indium tin oxide
PEDOT:PSS, poly(3,4-ethylenedioxythiophene):poly(styrenesulfonate)
THF, tetrahydrofuran
PL, photoluminescence
J–V, current density–voltage
XES, x-ray emission spectroscopy
XAS, x-ray absorption spectroscopy
AFM, atomic force microscopy
J_{sc}, short-circuit current
FF, fill factor
HOMO, highest occupied molecular orbital

■ REFERENCES

(1) Tang, C. W. *Appl. Phys. Lett.* **1986**, *48*, 183–185.
(2) Peumans, P.; Uchida, S.; Forrest, S. R. *Nature* **2003**, *425*, 158–162.
(3) Li, G.; Shrotriya, V.; Huang, J.; Yao, Y.; Moriarty, T.; Emery, K.; Yang, Y. *Nat. Mater.* **2005**, *4*, 864–868.
(4) Kim, J. Y.; Lee, K.; Coates, N. E.; Moses, D.; Nguyen, T.-Q.; Dante, M.; Heeger, A. J. *Science* **2007**, *317*, 222–225.
(5) Liang, Y.; Xu, Z.; Xia, J.; Tsai, S.-T.; Wu, Y.; Li, G.; Ray, C.; Yu, L. *Adv. Mater.* **2010**, *22*, E135–E138.
(6) Sun, Y.; Welch, G. C.; Leong, W. L.; Takacs, C. J.; Bazan, G. C.; Heeger, A. J. *Nat. Mater.* **2011**, *11*, 44–48.
(7) He, Z.; Zhong, C.; Huang, X.; Wong, W.; Wu, H.; Chen, L.; Su, S.; Cao, Y. *Adv. Mater.* **2011**, *23*, 4636–4643.
(8) Li, G.; Zhu, R.; Yang, Y. *Nat. Photonics* **2012**, *6*, 153–161.
(9) Xiao, X.; Wei, G.; Wang, S.; Zimmerman, J. D.; Renshaw, C. K.; Thompson, M. E.; Forrest, S. R. *Adv. Mater.* **2012**, *24*, 1956–1960.
(10) Clarke, T. M.; Durrant, J. R. *Chem. Rev.* **2010**, *110*, 6736–6767.
(11) Gregg, B. A.; Hanna, M. C. *J. Appl. Phys.* **2003**, *93*, 3605–3614.
(12) Gong, X.; Tong, M.; Brunetti, F. G.; Seo, J.; Sun, Y.; Moses, D.; Wudl, F.; Heeger, A. J. *Adv. Mater.* **2011**, *23*, 2272–2277.
(13) Ohkita, H.; Cook, S.; Astuti, Y.; Duffy, W.; Tierney, S.; Zhang, W.; Heeney, M.; McCulloch, I.; Nelson, J.; Bradley, D. D. C.; Durrant, J. R. *J. Am. Chem. Soc.* **2008**, *130*, 3030–3042.
(14) Peumans, P.; Yakimov, A.; Forrest, S. R. *J. Appl. Phys.* **2003**, *93*, 3693–3723.
(15) Erwin, P.; Thompson, M. E. *Appl. Phys. Lett.* **2011**, *98*, 223305.
(16) Yuan, Y.; Reece, T. J.; Sharma, P.; Poddar, S.; Ducharme, S.; Gruverman, A.; Yang, Y.; Huang, J. *Nat. Mater.* **2011**, *10*, 296–302.
(17) Nalwa, K. S.; Carr, J. A.; Mahadevapuram, R. C.; Kodali, H. K.; Bose, S.; Chen, Y.; Petrich, J. W.; Ganapathysubramanian, B.; Chaudhary, S. *Energy Environ. Sci.* **2012**, *5*, 7042–7049.
(18) Veldman, D.; Ipek, O.; Meskers, S. C. J.; Sweelssen, J.; Koetse, M. M.; Veenstra, S. C.; Kroon, J. M.; van Bavel, S. S.; Loos, J.; Janssen, R. A. J. *J. Am. Chem. Soc.* **2008**, *130*, 7721–7735.
(19) Deschler, F.; Da Como, E.; Limmer, T.; Tautz, R.; Godde, T.; Bayer, M.; von Hauff, E.; Yilmaz, S.; Allard, S.; Scherf, U.; Feldmann, J. *Phys. Rev. Lett.* **2011**, *107*, 127402.
(20) Engel, M.; Kunze, F.; Lupascu, D. C.; Benson, N.; Schmechel, R. *Phys. Status Solidi RRL* **2012**, *6*, 68–70.
(21) Hill, I. G.; Kahn, A.; Soos, Z. G.; Pascal, J. *Chem. Phys. Lett.* **2000**, *327*, 181–188.
(22) Knupfer, M. *Appl. Phys. A: Mater. Sci. Process.* **2003**, *77*, 623–626.
(23) Giebink, N. C.; Wiederrecht, G. P.; Wasielewski, M. R.; Forrest, S. R. *Phys. Rev. B* **2011**, *83*, 195326.
(24) Scholes, G. D.; Rumbles, G. *Nat. Mater.* **2006**, *5*, 683–696.
(25) Koster, L. J. A.; Shaheen, S. E.; Hummelen, J. C. *Adv. Energy Mater.* **2012**, *2*, 1246–1253.
(26) Camaioni, N.; Po, R. *J. Phys. Chem. Lett.* **2013**, *4*, 1821–1828.
(27) Van der Horst, J.-W.; Bobbert, P. A.; Michels, M. A. J.; Bässler, H. *J. Chem. Phys.* **2001**, *114*, 6950–6957.
(28) Leblebici, S. Y.; Catane, L.; Barclay, D. E.; Olson, T.; Chen, T. L.; Ma, B. *ACS Appl. Mater. Interfaces* **2011**, *3*, 4469–4474.
(29) Madigan, C. F.; Bulović, V. *Phys. Rev. Lett.* **2003**, *91*, 247403.
(30) Zhong, Y.; Ma, J.; Hashimoto, K.; Tajima, K. *Adv. Mater.* **2012**, *25*, 1071–1075.
(31) Watkins, P. K.; Walker, A. B.; Verschoor, G. L. B. *Nano Lett.* **2005**, *5*, 1814–1818.
(32) Heremans, P.; Cheyns, D.; Rand, B. P. *Acc. Chem. Res.* **2009**, *42*, 1740–1747.
(33) Piper, L. F. J.; Cho, S. W.; Zhang, Y.; DeMasi, A.; Smith, K. E.; Matsuura, A. Y.; McGuinness, C. *Phys. Rev. B* **2010**, *81*, 045201.
(34) Seo, J. H.; Kim, C. Y.; Kang, S. J.; Yoo, K.-H.; Whang, C. N.; Moewes, A.; Chang, G. S. *J. Chem. Phys.* **2007**, *126*, 064706.
(35) Wilks, R. G.; Chang, G. S.; Kim, K. H.; Choi, D. H.; Moewes, A. *J. Electron Spectrosc. Relat. Phenom.* **2011**, *184*, 355–359.
(36) Seo, J. H.; Jin, Y.; Brzezinski, J. Z.; Walker, B.; Nguyen, T.-Q. *ChemPhysChem* **2009**, *10*, 1023–1027.
(37) Brütting, W. In *Physics of Organic Semiconductors*; Brütting, W., Ed.; Wiley-VCH Verlag GmbH & Co. KGaA: Weinheim, Germany, 2006; pp 1–14.
(38) Angulo, G.; Grilj, J.; Vauthey, E.; Serrano-Andrés, L.; Rubio-Pons, Ò.; Jacques, P. *ChemPhysChem* **2010**, *11*, 480–488.